Composites: Part A 41 (2010) 612–623

Contents lists available at ScienceDirect

Composites: Part A

journal homepage: www.elsevier.com/locate/compositesa

Quantitative experimental measurements of matrix cracking and delamination using acoustic emission

Jonathan J. Scholey [a,b], Paul D. Wilcox [a,*], Michael R. Wisnom [b], Michael I. Friswell [c]

[a] Department of Mechanical Engineering, University of Bristol, BS8 1TR, UK
[b] Department of Aerospace Engineering, University of Bristol, BS8 1TR, UK
[c] School of Engineering, University of Swansea, SA2 8PP, UK

ARTICLE INFO

Article history:
Received 30 July 2009
Received in revised form 5 January 2010
Accepted 16 January 2010

Keywords:
D. Acoustic emission
D. Ultrasonics
B. Delamination
Matrix cracking

ABSTRACT

Quantitative measurements of the amplitude and angular variation of acoustic emission (AE) events due to matrix cracking and delamination in large quasi-isotropic composite plate specimens are reported. A procedure for determining the minimum specimen size necessary to make quantitative measurements is presented. The amplitude of AE events is quoted as the absolute surface displacement of different guided wave modes and can therefore be used as the input to forward models of the AE process. Matrix cracking events are found to be dominated by the S_0 guided wave mode and have a pronounced amplitude variation with angle. Events due to delamination growth are dominated by the A_0 guided wave mode and have no clear angular dependence.

1. Introduction

Acoustic Emission (AE) is the generation of transient waves due to the rapid release of strain energy from within a material, typically due to the occurrence of some type of damage. AE testing is the detection of damage via the detection of the elastic waves generated by an AE event. The high sensitivity of AE testing, coupled with its need for relatively few sensors make it an attractive technique for Structural Health Monitoring (SHM) systems. However, to achieve success in an SHM role, the performance of an AE system must be quantified [1] and, consequently, quantitative information about AE waveforms from the types of damage of interest must first be obtained.

This paper describes an experimental procedure for quantitatively characterizing the AE from damage mechanisms in planar composite material. For the first time measurements from different damage mechanisms are reported on an absolute displacement scale. The motivation for obtaining such measurements is to provide data for input into forward simulations of the AE testing process on more complex components and structures. Forward simulation models are necessary to quantify the performance of AE-based SHM systems. Such models simulate the response of one or more AE sensors to a particular type of damage at a certain location, and can be used for example, to estimate Probability Of Detection (POD) or to determine the optimum sensor placement.

The work conducted in AE testing is vast and a complete review of the literature is beyond the scope of this work. Thorough reviews are given by Hamstad [2] and Drouillard [3]. Hamstad describes four fundamental and repeated problems with AE source characterisation measurements reported in the literature:

- The failure to account for the effects of specimen geometry.
- The failure to account for the effects of propagation.
- The failure to account for the effects of AE system components.
- The failure to confirm the origin of AE events.

These problems lead to a case-specific results that are not transferable to general models. Notable exceptions to this include certain well-controlled experiments reported in the 1980s that used moment tensor analysis to invert experimental measurements to investigate the nature of certain AE sources, such as fatigue crack growth in an aluminium alloy [4] and thermal cracking in glass [5]. Also worthy of mention are so-called modal AE studies [6–9] where different modes of wave propagation are identified in the AE waveforms and used to characterize AE sources.

With the exception of specimen geometry, most of the problems listed by Hamstad have been independently addressed in the literature. To include the effect of propagation, Scholey et al. [10] used a linear time-invariant (LTI) systems approach [11] to simulate dispersion, attenuation and reflection or transmission, using data from AE source characterisation experiments as an input. To account for AE system components, a variety of techniques for calibrating AE sensors are available in the literature including

* Corresponding author. Tel.: +44 117 928 9752.
E-mail address: p.wilcox@bristol.ac.uk (P.D. Wilcox).

1359-835X/$ - see front matter © 2010 Elsevier Ltd. All rights reserved.
doi:10.1016/j.compositesa.2010.01.008

variations on the ASTM standard approach [12,13] and the reciprocity technique [14]. To determine the origin of AE events, source location based on triangulation from the arrival times of individual wavepackets on multiple sensors can be used. Such localisation tools are well established for isotropic plates [15] and have also been demonstrated for anisotropic plates [16,17].

The problem that has received the least attention is that of specimen geometry. The vast majority of laboratory-based AE source characterisation has been conducted on narrow plate coupons where the AE source and sensors are necessarily located close to the specimen edges. Plate edges reflect elastic wave energy back into the specimen [18,20] which interferes with the waveform propagating directly from the source to the sensor. The amount of interference depends on the propagation properties of the elastic waves, the experimental layout and the exact source location, which often cannot be precisely controlled. There is no simple technique for removing the effects of reflected wave energy from AE waveforms in small specimens and, as a result, it is very difficult to separate the effects of specimen geometry from the AE source information. Furthermore, real AE sources do not radiate energy uniformly in all directions [4,5], but this angular variation cannot be observed if narrow specimens are used. Hamstad suggested the obvious solution of using large specimens to allow reflection-free measurements of the directly emitted waves from an AE source [18]. However, experiments on large specimens are less attractive than those on small specimens: larger loads are necessary to generate damage, special measures must be taken to ensure damage occurs at the desired location (i.e. in the center of the specimen rather than at the edges) and larger specimens are more expensive. For these reasons, there have been almost no reported quantitative source characterisation measurements on large specimens and, to the best of the authors' knowledge, none have been reported on fibre reinforced composite samples.

In this paper, plate (rather than bulk specimens) are used because they are representative of the basic structural element of many real composite structures on which an AE-based SHM might be deployed. In plates, the AE signals propagate away from the source as guided waves, which are by their nature multi-modal and dispersive [19]. It should be stressed that the experimental methodology described in this paper is for the purpose of source characterisation only; it should not in any way be regarded as the required design for an SHM application. The results from the source characterisation experiments described here are intended to be used to provide the input for models of AE in more complex structures. Such models can readily account for reflection and transmission of AE signals past multiple structural features, enabling robust simulations of the AE process in complex structural components.

Section 2 describes the design of composite plate specimens with sufficiently large in-plane dimensions to enable accurate measurements of the amplitude of directly emitted guided waves from two different damage mechanisms. The experimental procedure and the calibration of the experimental hardware to absolute surface displacement for different guided wave modes are described in Section 3. The results are presented in Section 4 and discussed in Section 5.

2. Experimental specimens

2.1. Plate lay-up

The plates used here were manufactured at the University of Bristol from AS4/8552 pre-preg material with lay-up $[(+45, 90, -45)_2, 0_2]_s$. The material properties, in-plane elastic modulae (E_1 and E_2), in-plane shear modulus (G_{12}) and in-plane Poisson's ratio (υ_{12}), of the AS4/8552 ply material are taken from [21] and are listed in the Appendix A. For the transverse Poisson's ratio (υ_{23}) a value of 0.45 is used. Using classical laminate theory, it can be shown that this lay-up results in a plate with isotropic in-plane extensional and shear stiffness. A nominal ply thickness of 0.125 mm gave an overall plate thickness of 2 mm.

2.2. Determination of guided wave properties

Fig. 1 shows the group velocity dispersion curves for the two propagating modes measured on a large 2 mm thick plate with the above lay-up. The measurement was made using a phase-delay technique [10,22], where a laser interferometer was used to measure the change in-phase of wavepackets in two waveforms recorded at different points on a ray-path. The experimentally-measured group velocity dispersion curve was compared with a numerical solution obtained using *DISPERSE* (Imperial College, London) software [23]. The laminate stiffness values used in *DISPERSE* are reported in the Appendix A. These are the equivalent homogenous properties calculated from the properties of individual lamina, which are also listed in the Appendix A. At 250 kHz, the variation in-phase and group velocity of the fundamental guided wave modes A_0 and S_0 with angle is negligible (<0.1 %). The agreement between the experimental and theoretical group velocity is excellent and was found to be similar in all propagation directions. The plates can therefore be regarded as quasi-isotropic as far as the propagation of the fundamental guided wave modes is concerned.

2.3. Specimen size calculation

With knowledge of the guided wave velocities, it is possible to design the specimen geometry. A simple approach for visualizing the dispersion of elastic waves along a single ray-path was described by Wilcox et al. [24]. Here, that technique is extended for visualizing the interaction of dispersive wavepackets propagating in a two-dimensional plate structure through the use of a location–time plot. The basic concept is to plot the trajectory of wave packets along the ray-paths of interest in three-dimensions (3D), where two of the dimensions represent the in-plane spatial position within the plate and the third-dimension represents time. In a plate, an AE source generally radiates energy in all in-plane directions, but the ray-paths of interest here are only those that ultimately reach the sensor. In terms of specimen design, the most important ray-paths are: (a) the path directly from the source to the sensor and (b) the shortest ray-path from the source to the sensor with a single reflection from a specimen boundary. Wavepackets that propagate along these ray-paths to the sensor are

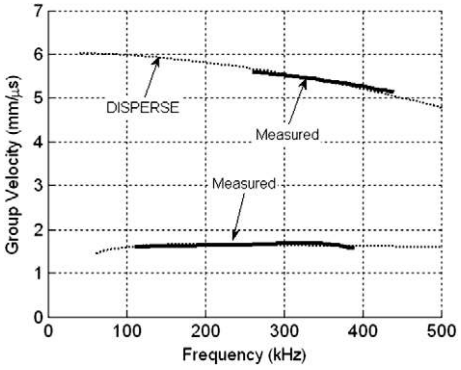

Fig. 1. Group velocity dispersion curves in the 0° ply direction for a 2 mm thick AS4/8552 plate. The upper curve is the fundamental symmetric mode, S_0, and the lower curve is the fundamental anti-symmetric mode, A_0.

referred to as direct and reflected wavepackets, respectively. The direct wavepackets are those that will be used to characterise the source. The reflected wavepackets are important in that it must be ensured, as far as possible, that they do not interfere with the direct wavepackets of interest. The location–time plot enables relatively simple equations to be written for the temporal start and end of each wave-packet arrival at a sensor, and consequently the minimum specimen size in order to avoid wave-packet overlap can be determined. The technique can also be extended to anisotropic plates where the wave velocity is a function of angle, although this is not the case here as shown previously.

It is assumed that a square plate specimen is used, and that the AE source occurs at the center of the specimen. At each sensor location, the objective is therefore to resolve the direct wavepackets of different guided wave modes both from one another and from reflected wavepackets. Separation of the direct wavepackets from one another implies that sensors must be more than a certain critical distance away from the source. Because the velocity profile of both modes is isotropic in this case, the locus of minimum critical distance is a circle around the center of the plate. In terms of resolving direct wavepackets from reflected wavepackets, it can be seen by inspection (again because the velocity profile is isotropic) that the critical angular positions of sensors are at 0°, 90°, 180° and 270° with respect to the plate axes.

Fig. 2 shows a location–time plot of the wavepackets from an AE event occurring at the center of a 400 mm square plate with the properties previously described. Because of symmetry, only a quarter of the plate is modeled and the AE event occurs at the spatial location $X = 0$, $Y = 0$ in the location–time plot. The size of plate and sensor position in the location–time plot in Fig. 2, represents the 400 × 400 mm measurement area of the actual experimental specimens used here, although in the following discussion it is used simply to illustrate the specimen geometry calculation procedure. The figure shows the trajectory of wave packets along three ray-paths that arrive at a sensor location (75 mm, 0). The first is from the AE source location (0, 0) directly to the sensor; the second is a continuation of this ray to the boundary of the active area at (200 mm, 0) where it is reflected back to the sensor; the third is that of waves reflected off the other boundary at (37.5 mm, 200 mm). In order to compute these trajectories, various pieces of information about the AE source and wave propagation in the plate are needed. The gradient of the lines describing the lower (i.e. earlier) temporal boundary of each wavepacket are defined by the fastest group velocity of the particular guided wave mode over the bandwidth of the AE source. Similarly, the gradient of the lines describing the upper (i.e. later) temporal boundary are defined by the slowest group velocity of the guided wave mode over the bandwidth of the AE source. The lower and upper temporal bounds are offset at the location of the AE source by its temporal duration.

From the preceding description of the location–time plot constructions, it appears to be necessary to have *a priori* knowledge of the bandwidth and temporal duration of the AE source. However, the authors postulate that individual physical phenomena responsible for AE events themselves, such as the sudden advance of a crack front or a stick/slip event in a delamination, happen over such short time-scales that their temporal profiles can be regarded for practical purposes as delta function-like. The implication of this is that the bandwidth of the wavepacket measured at a sensor is determined by other factors. These include, the frequency-dependent excitability of different guided wave modes, the attenuation incurred by the guided waves *en route* to the sensor and, most significantly, by the frequency response function of the sensor and instrumentation. Therefore, the parameters required for the distance–time plot are the bandwidth and temporal duration of the impulse response of a sensor and instrumentation. In the work described here, the sensors are relatively broadband, and the bandwidth is intentionally limited by a digital band-pass filter. This is applied in post-processing in the frequency-domain and has a precisely specified frequency profile, and hence impulse response. The bandwidth is defined by a raised cosine function spanning the frequency range from 50 kHz to 450 kHz, and the corresponding impulse response has a duration of $T = 20$ μs. Note that although this represents the temporal duration of an impulse applied directly to the sensor, it can be regarded equivalently as the temporal duration of the AE source, which is more useful for the purposes of constructing the location–time plot. Over the bandwidth 50–450 kHz, the minimum and maximum velocities of the A_0 guided wave mode are $v^{\min}(A) = 1.5$ mm μs^{-1} and $v^{\max}(A) = 1.6$ mm μs^{-1}, and those of the S_0 guided wave mode are $v^{\min}(S) = 5.0$ mm μs^{-1} and $v^{\max}(S) = 6.0$ mm μs^{-1}. From the location–time plot, it can easily be deduced that the minimum radial distance, $r_{\min}$, at which the directly emitted wavepackets are resolved in time is given by:

$$r_{\min} = T\frac{v_{\min}^{(S)} v_{\max}^{(A)}}{v_{\min}^{(S)} - v_{\max}^{(A)}}. \tag{1}$$

For the specimen and instrumentation considered here, this evaluates to 47 mm. To ensure complete temporal separation of the direct wavepackets from the first reflections, the minimum size of plate, $L_{\min}$, can be computed:

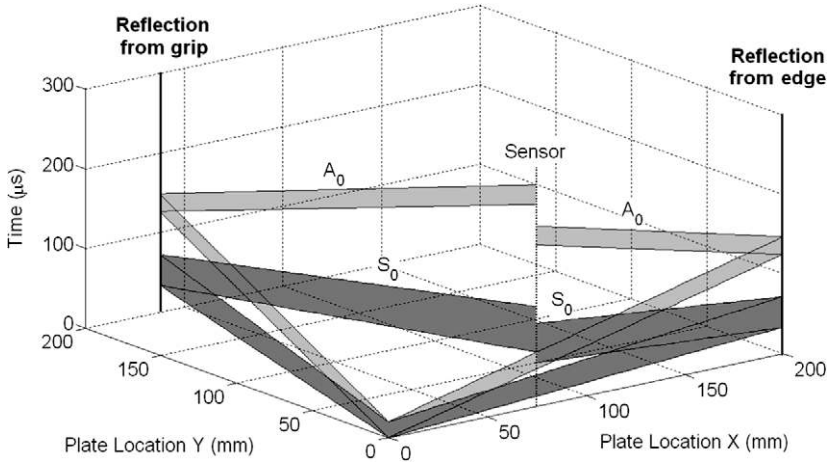

Fig. 2. Location–time plot of guided waves emitted from AE source at (0, 0) on AS4/8552 lay-up $[(45, 90, -45)_2, 0_2]_s$ plate.

$$L_{\min} = v_{\max}^{(S)} T + r_{\min}\left(1 + \frac{v_{\max}^{(S)}}{v_{\min}^{(A)}}\right), \quad (2)$$

which for the system here is 355 mm. Because the location of AE sources due to damage cannot be precisely controlled, this size should be regarded as an absolute lower bound only.

In the experimental work described here, the authors elected to increase the tolerance on source location uncertainty by placing sensors on a circle with a radius of 75 mm, which corresponds to the sensor position indicated in Fig. 2. However, this sensor position is now too close to the specimen edge to allow complete separation of the direct A_0 wavepacket from the first S_0 reflection. This limitation is accepted on the basis that the direct wavepacket of most interest is the dominant mode. If the dominant mode in the first arrival is the A_0 mode, then this is also likely to dominate the reflected S_0 mode wavepacket. This is because although the S_0 mode has a somewhat lower attenuation than the A_0 mode, the first S_0 mode reflection has to propagate more than four times further than the direct A_0 mode wavepacket. Of course, if the direct wavepacket is S_0-dominated there is no problem as the direct S_0 wavepacket is fully resolvable from other wavepackets.

3. Experimental procedure

3.1. Specimen manufacture

Four 600 mm x 400 mm plates were manufactured at the University of Bristol from AS4/8552 pre-preg material with the properties and lay-up described previously. The specimens were cured in an autoclave using the manufacturer's recommended cure cycle at 180 °C under a pressure of 7 Bar (Hexcel, Duxford, UK). Aluminium end tabs, measuring 100 × 400 mm were bonded to the plate using Hexcel Redux-A two part epoxy. The epoxy was cured for 1 h at 70 °C under a pressure of 7 Bar.

AE waveforms were monitored at four locations a distance of 75 mm from the center of the plate as shown in Fig. 3. The sensor locations were chosen to allow the measurement of angular amplitude patterns (using sensor locations 1–3) and to facilitate source location via triangulation using sensor locations 1–4. The sensors used in this work were manufactured in the University of Bristol NDT laboratory. The main component of the sensor is an undamped cylindrical pz-27 lead zirconate titanate (PZT) piezo-ceramic element (Ferroperm, Kvistgard, Denmark) with a diameter of 3 mm and a height of 3 mm. At each sensor location shown in Fig. 3, two sensors were bonded using commercial cyanoacrylate adhesive at collocated points on opposite sides of the plate. This enabled the propagating mode to be identified using the technique described in Section 3.5.

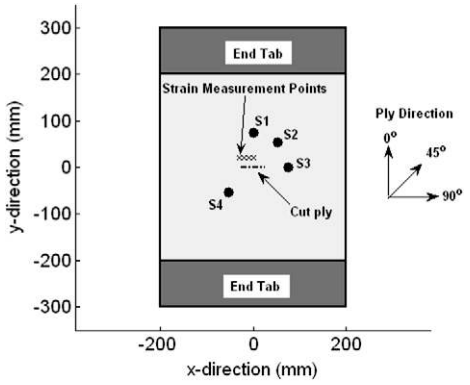

Fig. 3. Plate specimen geometry. The sensor locations in mm with respect to the center of the cut-ply are: S1 (0, 75); S2 (53.03, 53.03); S3 (75, 0); and S4 (-53.03, -53.03).

3.2. Damage mechanism

Artificial discontinuities were introduced at the center of the plates by making a cut through the central block of 0° plies, perpendicular to the fibre direction. The cuts were made using a knife during the lay-up of the specimen. Three of the four specimens contained cut plies of different lengths which are summarized in Table 1. Earlier investigations of cut plies indicated that this was a simple way to introduce a localized delamination region into a plate [25,26].

Fig. 4 shows a cross-section of a cut-ply region after loading, with damage features highlighted using penetrant UV dye. The cut-ply can be seen to open and form a vertical crack spanning the block of 0° plies. Two delamination regions, seen as horizontal cracks at the interface of the 0° plies and 45° plies, extend from the cut-ply. The opening of the cut-ply is perpendicular to the loading direction and as a result, has similarities with Transverse Matrix Cracking (TMC) events. However, the opening of the resin rich region inside the buried crack is not strictly TMC and is referred to as matrix cracking in this work.

3.3. Loading procedure and strain measurement

Three of the four plates were loaded in quasi-static tension in a Dartec 500 kN servo-hydraulic testing facility at a rate of 2 mm min^{-1}. A summary of the loading conditions of the three specimens is shown in Table 1. The strain was monitored on opposite sides of the plate at four locations using a video extensometer [27] (Imetrum, Bristol, UK). The reported strain values throughout this work are the average of the measurements made at the four locations. Because the video extensometer is non-contact, it does not interfere in any way with the AE measurements. The locations of the strain measurements are shown in Fig. 3.

Table 1
Defect and loading details of plate specimens.

Specimen	Cut-ply length (mm)	Maximum load (kN)	Maximum strain (%)
DL-L-50	50.0	235	0.738
DL-L-25	25.0	232	0.735
DL-L-12	12.5	251	0.810
DL-L-00	0.0	~	~

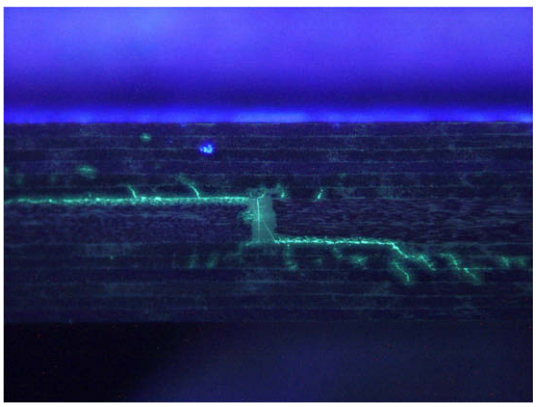

Fig. 4. Examination of cut-ply region after loading using UV penetrant dye analysis.

3.4. AE system hardware

The eight pz-27 sensors were connected to PAC 2/4/6 pre-amplifiers (Physical Acoustics Corporation, Princeton Junction, NJ) which were connected to an 8-channel PAC PCI-2 data acquisition unit. The nominal pre-amplifier gain was fixed at 40 dB.

A hit is a waveform recorded on a single channel by the AE system when the waveform amplitude exceeds some threshold amplitude. The triggering point is defined as the time at which the hit waveform first exceeds a certain threshold amplitude. The threshold amplitude was set a few dB above the ambient noise level and was between 48 dB_{ae} and 52 dB_{ae} for all tests. It should be noted that no hardware filtering was applied during testing. The calibration of the AE system hardware is described in Section 3.7.

3.5. Post-processing

A code, written in *MATLAB*, was used to screen, filter and interpret the raw waveforms. The code initially screens the raw waveforms and discards those that fall below a specified threshold value. Raw waveforms from different sensors with triggering points that occur within a specified time window of each other are then considered to correspond to an AE event. For the results which follow, the time window which was used to link raw waveforms into events was 100 μs.

The raw waveforms due to each event are then filtered in the frequency-domain. An important characteristic of the pz-27 sensors is that they have a reasonably flat frequency response below their first resonant frequency, making them ideal for quantitative measurements in this range. The Fourier transform of each waveform is multiplied by a raised cosine filter with a center-frequency of 250 kHz and bandwidth of 400 kHz. This ensures that data outside this range (which at lower frequencies is contaminated by acoustic noise and at higher frequencies is distorted by the first sensor resonance and higher order guided wave modes) is removed. When the filtered spectra are inverse Fourier transformed, the resulting waveforms have a well-defined bandwidth and center-frequency of 250 kHz. This is important for subsequent source location, where the velocity of a wavepacket is required. The wavepacket velocity can now be unambiguously defined as the group velocity of the appropriate guided wave mode at the center-frequency of 250 kHz.

The propagating mode at the triggering point is identified by examining the relative phase of the filtered waveforms recorded on a pair of collocated sensors. Waveforms which are in-phase at the triggering point indicate triggering by the S_0 mode while those in anti-phase indicate the A_0 mode. Note that the propagating mode at the time of triggering is not necessarily the dominant mode in the waveform; the identification of the triggering mode is purely to enable the correct modal velocity to be used in localizing the source.

3.6. Source location

Source location was conducted using the best-matched point search method [17]. The best-matched point search method works by comparing the difference in triggering time of experimental waveforms measured at different sensor locations, known as delta-t values, with a set of theoretical delta-t values calculated at different points on the test geometry based on the known guided wave velocities. The location of the AE source is given by the point which has the closest match between experimental and idealized delta-t values. Identification of the propagating mode at the triggering point of experimental waveforms enables the correct value of group velocity to be used in the source location algorithm. The velocities used to calculate the idealized delta-t values for the S_0 and A_0 modes are 5.60 mm μs^{-1} and 1.60 mm μs^{-1}, respectively. These velocities correspond to the group velocities of the two modes in the AS4/8552 plate at 250 kHz (the center-frequency of the band-pass filter). Since the plate is quasi-isotropic the specified velocities are applicable in all directions.

3.7. Experimental calibration

In order to obtain quantitative source characterisation data, it is necessary to calibrate the voltage of a recorded AE waveform to the absolute surface displacement of a specified guided wave mode. Practically, this means finding the transfer function of each component in the measurement system. The measurement system includes the sensors, amplifiers and filters. The gain of the PAC 2/4/6 pre-amplifiers was measured and found to be 44 dB when set to a nominal 40 dB gain. All filters in the PAC PCI-2 system were disabled (this was verified by comparing trial waveforms recorded in parallel on the PAC system a LeCroy 6030 digital storage oscilloscope). The only remaining component requiring calibration is therefore the sensor itself and the procedure for doing this is summarized below.

There are several approaches reported in the literature for determining the sensor transfer function including the ASTM approach [12] and reciprocity technique [14]. In this work, a modified version of the ASTM approach was used which allows *in situ* calibration using a Polytec OFV-505/2700 laser vibrometer system to obtain an absolute displacement measurement [13]. The procedure uses a repeatable reference source (in the form of another pz-27 transducer connected to a signal generator) temporarily bonded to the surface of the plate at the intended damage location. Prior to installation of a monitoring sensor pair, the surface displacement at the sensor locations is recorded using the laser vibrometer when the reference source is excited with a suitable signal (i.e. a toneburst with the desired bandwidth). The sensor pair is then installed without disturbing the reference source and waveforms from both sensors are recorded when the reference source is excited with the same signal. The calibration is conducted independently for both the S_0 and A_0 guided wave modes, which are resolvable in the time-domain, as the transfer function depends on parameters that are both mode- and frequency-dependent such as mode-shape and wavelength in addition to just frequency. Although the sensor transfer function for each mode is strictly frequency-dependent it may, in practice, be approximated by its value at a single frequency. These scalar values only convey amplitude information and, as a result, any phase change due to the sensor is discarded. At 250 kHz (the center-frequency of the bandpass filtered applied later in post-processing), a typical calibration value was around 0.5 pm V^{-1} for both the A_0 and S_0 modes. It should be stressed that separate calibration values are obtained for each mode at each sensor in the experiment.

4. Experimental results

The experimental results are reported in two stages. Firstly, source location is performed and used to confirm the origin of the source and likely damage mechanism. Afterwards, the source characteristics of matrix cracking and delamination are examined. It should be noted that unless stated, the waveforms shown in the figures are randomly selected from the relevant data sets.

4.1. Source location

Source location is used to confirm that each acoustic source originates in the region of damage (rather than for example at the points

where the specimens are gripped). This therefore provides increased confidence that the results are from genuine events related to the damage.

Example source location results are shown for Specimen DL-L-50. Specimen DL-L-50 contained a 50 mm cut-ply and was loaded in quasi-static tension to 0.74% strain (235 kN). An independent measurement of the damage area was made before and after loading to provide a comparison with the source location results. Ultrasonic C-scans taken before and after testing are shown in Fig. 5a and b, respectively. Before loading a resin rich region around the cut plies can be seen. After loading an extensive damage area exists at the center of the plate. The damage area is a little wider than the initial 50 mm cut and has advanced, as expected, in the loading direction.

Source location was used to generate cumulative event plots which describe the total number of events that occur at each point during the test. Only events where all sensor pairs triggered on the same mode are considered; events where triggering occurred on mixed modes were generally of low amplitude and mode identification was unreliable. The points used in the source location algorithm and cumulative event plots had a resolution of 2 mm. The cumulative event plot for loading up to 0.37% strain is shown in Fig. 6a. The agreement between the estimated event location and the location of the cut-ply, shown in Fig. 5a and highlighted by the dotted line in Fig. 6a, is reasonable, with most events being localized to within a few mm of the cut. With the exception of one event, all events occur between 0.16% and 0.17% strain and are attributed to cracking of the resin rich region between the cut plies.

Between 0.37% strain and 0.74% strain 118 events were recorded; 95 events were triggered on the S_0 mode, 2 on the A_0 mode and the remaining 21 were triggered on mixed modes. The cumulative event plot for loading between 0.37% and 0.74% strain is shown in Fig. 6b and shows a much more extensive spread of locations than that at 0.37% strain. The agreement between the estimated event location and the location of the damage area identified by the C-scan is excellent. All of the recorded events occur above 0.55% strain and based on their estimated location are assumed to correspond to the initiation and propagation of delamination. It should be noted that specimens DL-L-25 and DL-L-12 showed similar agreement between source location plots and C-scan measurements.

4.2. Matrix cracking characteristics

All three specimens demonstrated similar AE characteristics. In tensile loading between 0.15% and 0.20% strain, multiple AE events occurred and were located within a few mm of the cut-ply. These

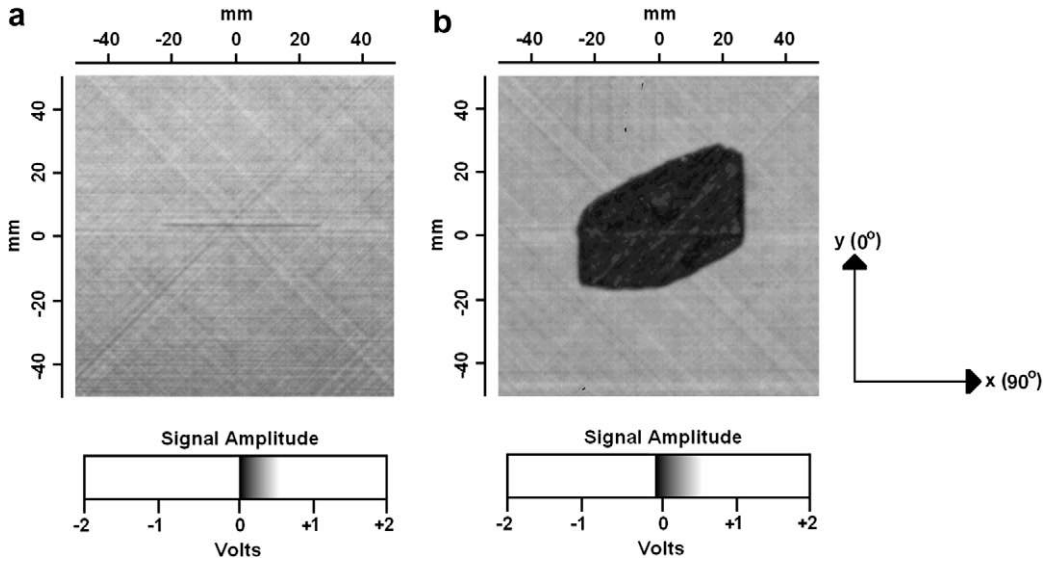

Fig. 5. C-scan of specimen DL-L-50: (a) before loading and (b) after loading.

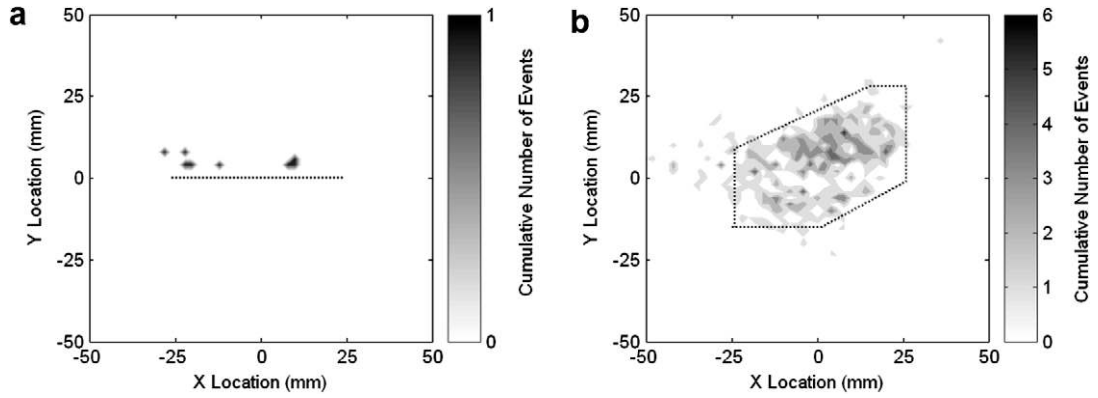

Fig. 6. Cumulative number of events at each location during the static test of specimen DL-L-50 for: (a) 0.00–0.37% strain and (b) 0.37–0.74% strain.

events were attributed to the cracking of the resin rich region and their characteristics are discussed here. The reported characteristics are taken from specimen DL-L-12 which had a cut-ply length of 12.5 mm. The small cut-ply meant that the propagation distance to each sensor location was approximately equal removing most of the possible variation due to differences in propagation distance.

In the loading of specimen DL-L-12, 18 events were recorded between 0.17% and 0.20% strain. The variation in overall amplitude of the events from matrix cracking is examined in Fig. 7, where four randomly-selected matrix cracking waveforms measured at sensor location 1 are compared. In the early part of the waveform, the waveforms measured on opposite sides of the plate are in-phase and, as a result, indicate S_0 mode propagation. Since this mode dominates the received waveforms the vertical scale in this figure is based on the calibration for the S_0 mode. The amplitude variation between events is quite large and, when considering all 18 events, there is an amplitude variation of approximately 16 dB. There is some evidence of the A_0 mode approximately 35 μs after the first arrival of the S_0 mode. The arrival of an A_0 at this time was predicted by the location–time plot and corresponds to the A_0 mode propagating directly between the source and sensor.

The angular amplitude pattern of the matrix cracking events was examined by comparing the waveforms measured at sensor locations 1–3 for each individual matrix cracking event. Typical waveforms for one randomly-selected matrix cracking event are shown in Fig. 8a–c, respectively. The received waveforms are dominated by the S_0 mode (i.e. the wavepacket that arrives first) in all three propagation directions. For this event, the absolute amplitude of the S_0 mode in the 0° ply direction is almost 100 pm (pm = picometers) and in the 90° ply direction is approximately 10 pm. The difference in amplitude in the different directions is quite large and indicates that this type of event has a pronounced angular amplitude pattern.

The mean, range and standard deviation of the absolute amplitude measurements of the matrix cracking events, measured in the three propagation directions for specimens DL-L-12 and DL-L-25, are summarized in Fig. 9a. Fig. 9b shows the angular amplitude pattern obtained by normalizing the amplitude of each event by that in the 0° propagation direction for specimen DL-L-12. It can be seen that the surface displacement varies by about 20 dB over the range of measurements. The error bars indicate the range of the normalized amplitudes measured at each angular location and show that for matrix cracking events, the angular amplitude pattern is remarkably consistent.

4.3. Delamination

In the loading of the large specimens, many events were reported after 0.55% strain. Above this strain, the source location of events indicated that delamination was advancing from the cut-ply in the loading direction. The characteristics of the delamination events reported here are taken from specimen DL-L-12 which had a cut-ply length of 12.5 mm. Again, the small cut-ply meant that the propagation distance to each sensor location was approximately equal, reducing variation due to differences in propagation distance.

Fig. 10a–d compares the surface displacement measured at sensor location 1 for four randomly-selected delamination events. In all events, the A_0 mode (i.e. the second wavepacket to arrive in the waveforms in Fig. 10) is dominant and, as a result, the vertical scale of the received waveforms is calibrated for the A_0 mode. These waveforms differ greatly from the matrix cracking waveforms which were dominated by the S_0 mode. There is some

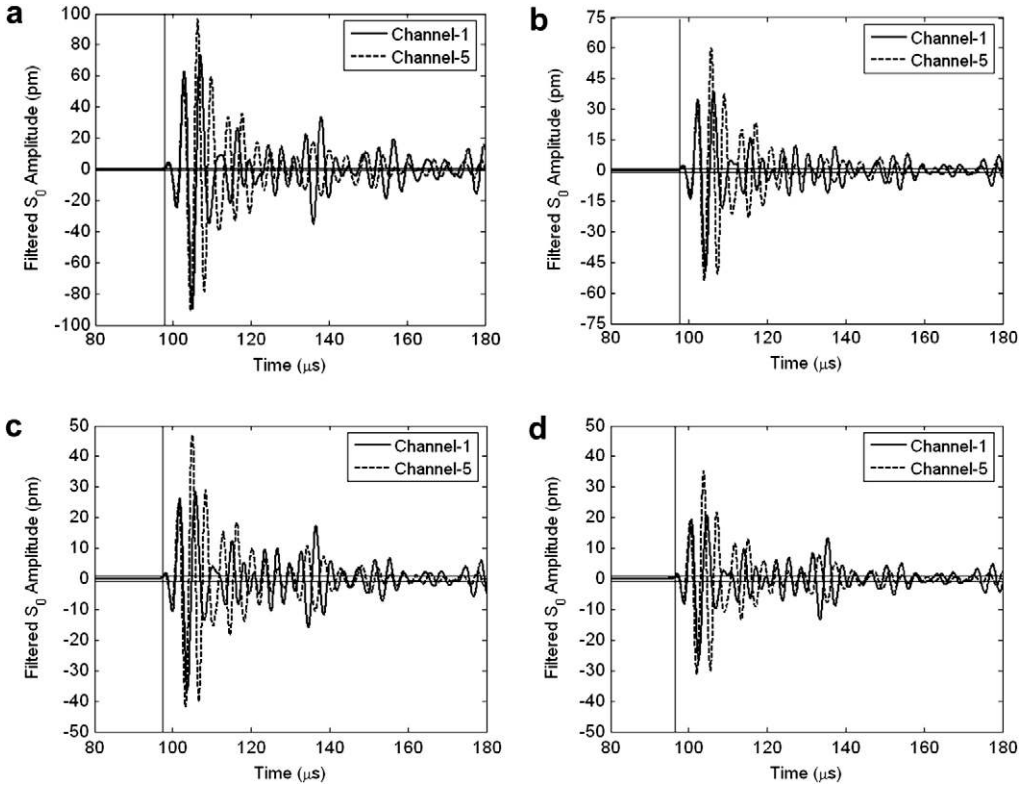

Fig. 7. Four example waveforms for matrix cracking events after filtering measured at sensor location 1 during the quasi-static loading of specimen DL-L-12: (a) event 1; (b) event 2; (c) event 3; and (d) event 4. Solid horizontal lines indicate the threshold amplitude; solid vertical lines indicate the trigger time. The waveforms immediately after the trigger time are clearly in-phase for each pair of sensors indicating S_0-triggered waveforms. This wavepacket is also the dominant one, indicating an S_0-dominated event.

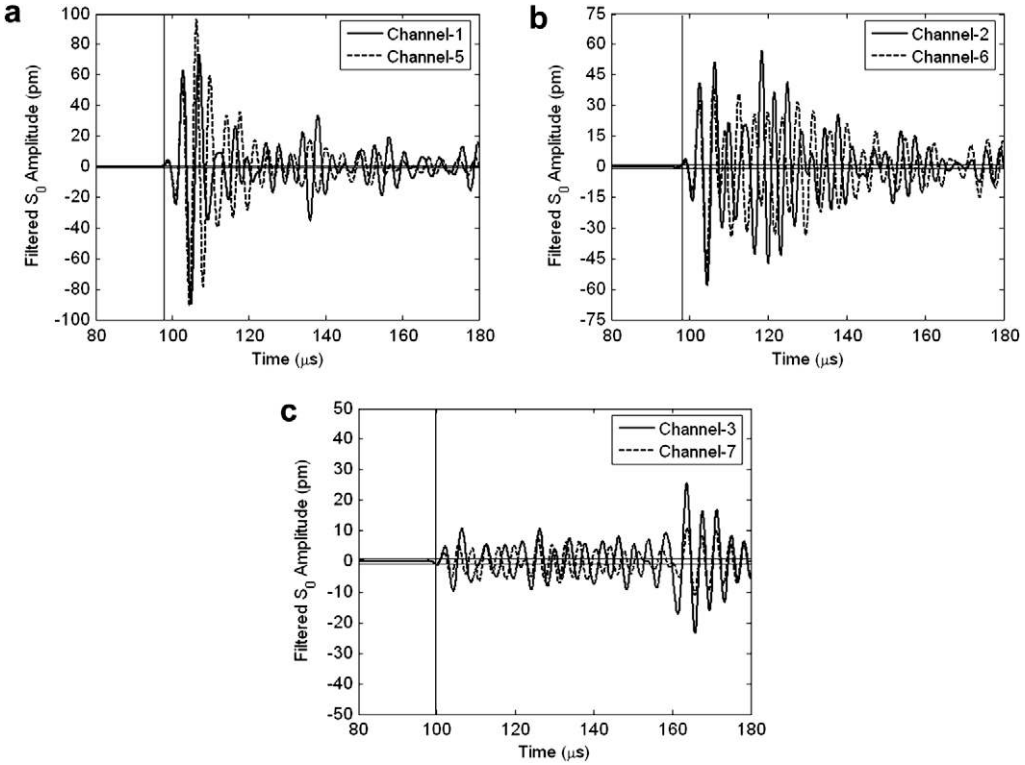

Fig. 8. Three example waveforms for the same matrix cracking event after filtering measured at different sensor locations during the quasi-static loading of specimen DL-L-12: (a) location 1; (b) location 2; and (c) location 3. Solid horizontal lines indicate the threshold amplitude; solid vertical lines indicate the trigger time.

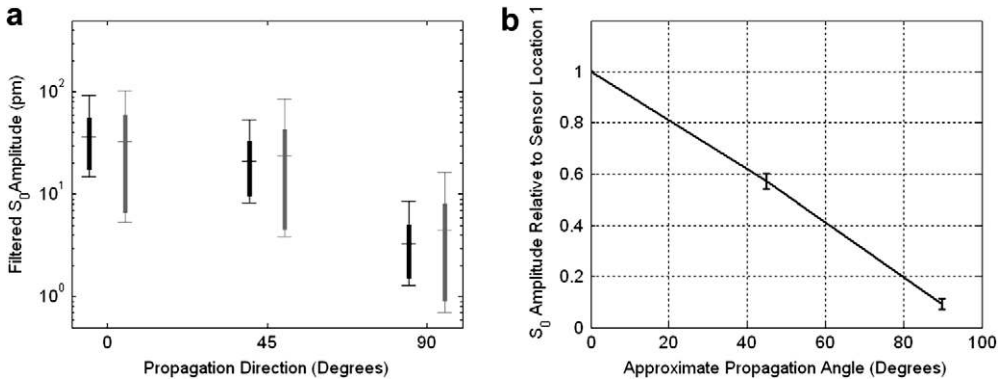

Fig. 9. Angular amplitude patterns from matrix cracking events: (a) mean amplitude, amplitude range and standard deviation of waveforms from specimen DL-L-12 (black bars) and DL-L-25 (grey bars) and (b) results from specimen DL-L-12 with amplitude normalized to the 0° propagation direction.

variation between the amplitude of the events, and when considering all delamination events the variation is approximately 40 dB.

It can be seen that the A_0 mode arrives approximately 30 μs after the S_0 mode, as predicted by the location–time plots. As noted previously, the location–time plots predict that the A_0 mode is contaminated by the first reflection of the S_0 mode. However, since the S_0 mode amplitude is much smaller than the A_0 mode, and will lose further amplitude over the additional distance traveled, it is not thought to affect the A_0 amplitude significantly.

The angular amplitude pattern of a delamination event was examined by comparing the waveforms measured at sensor locations 1–3 for a each event. Example waveforms for one particular event are shown in Fig. 11a–c, respectively. In all three propagation directions it can be seen that the propagation is dominated by the A_0 mode. For this event, the absolute amplitude of the A_0 mode in the 0° ply direction is almost 50 pm and in the 90° ply direction is approximately 15 pm. The difference in amplitude in the different directions is quite large and indicates the presence of an angular amplitude pattern for an individual event, albeit one that is less significant than that of the matrix cracking events.

The mean, range and standard deviation of the absolute amplitude measurements of the delamination events, measured in the three propagation directions for specimens DL-L-12 and DL-L-25, are summarized in Fig. 12a. The vast majority of events due to delamination are low amplitude, with an absolute surface displacement much below the average shown on the plot. However, the presence of a few very large events misleadingly distorts both the average and standard deviation. Thus, the average and standard deviation are calculated with the 10 largest amplitude events removed. The 10 events with the largest amplitude are shown on

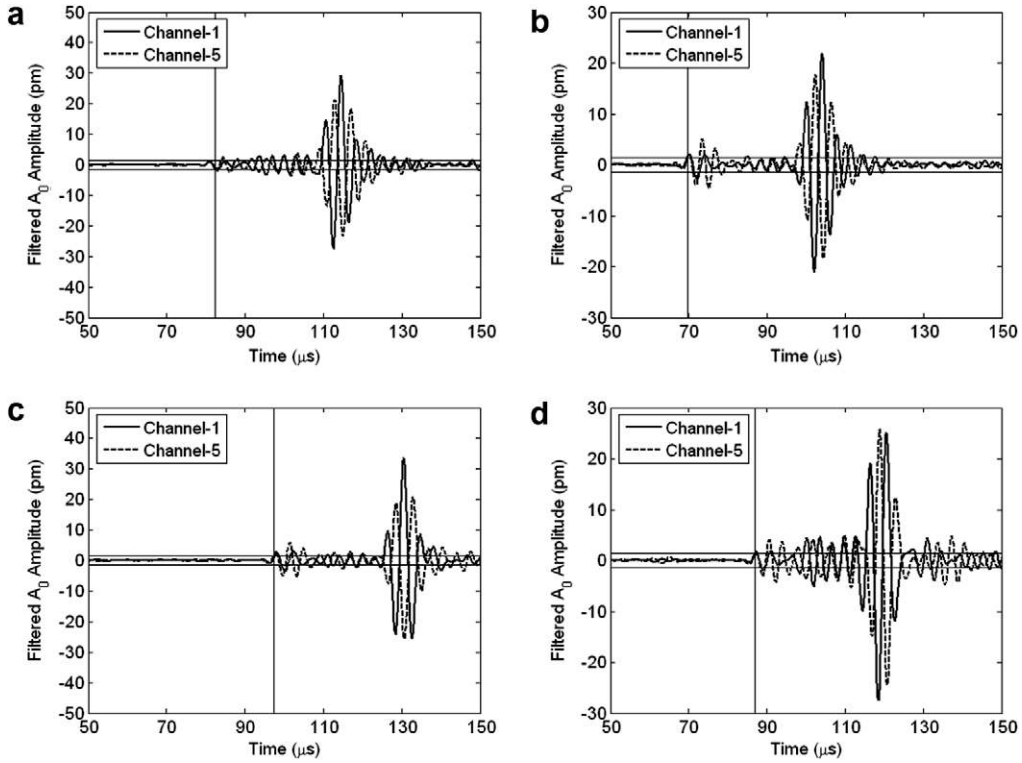

Fig. 10. Four example waveforms for delamination events after filtering measured at sensor location 1 during the fatigue loading of specimen DL-L-12: (a) event 1; (b) event 2; (c) event 3; and (d) event 4. Solid horizontal lines indicate the threshold amplitude; solid vertical lines indicate the trigger time. The waveforms immediately after the trigger time are clearly in-phase for each pair of sensors indicating S_0-triggered waveforms. However, the dominant wavepacket is now some time after the trigger point. Within the dominant wavepacket, it can be seen that the waveforms from each sensor pair are in anti-phase, indicating that the event is A_0-dominated.

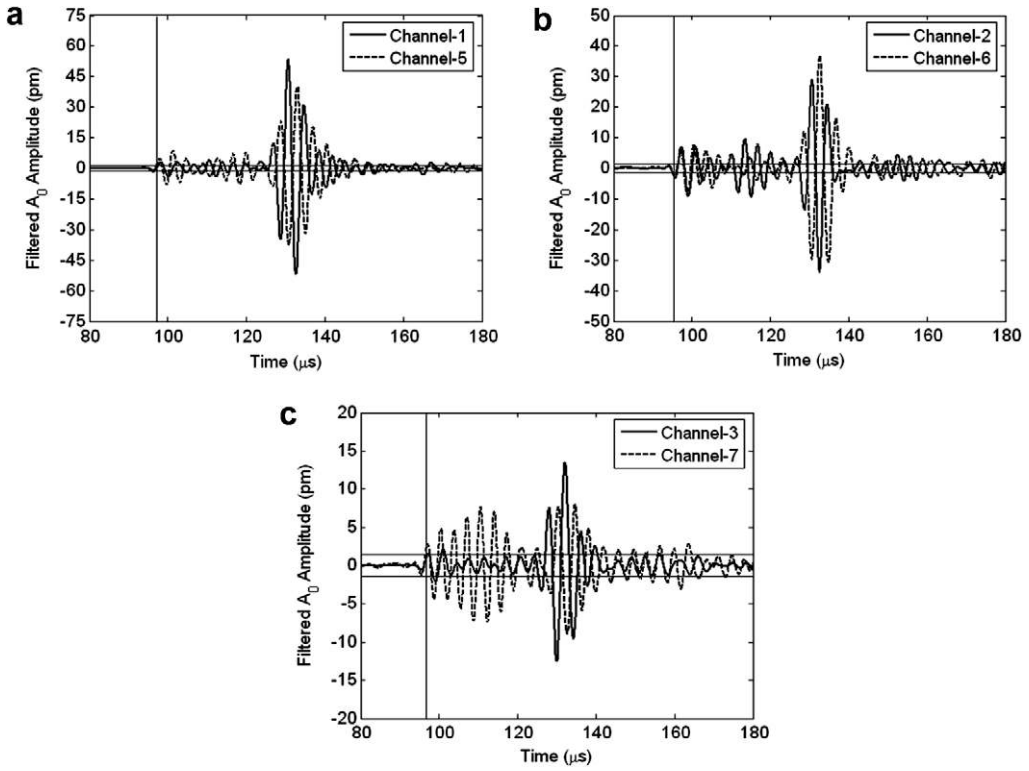

Fig. 11. Three example waveforms for the same delamination event measured at different sensor locations during the quasi-static loading of specimen DL-L-12: (a) location 1; (b) location 2; and (c) location 3. Solid horizontal lines indicate the threshold amplitude; solid vertical lines indicate the trigger time.

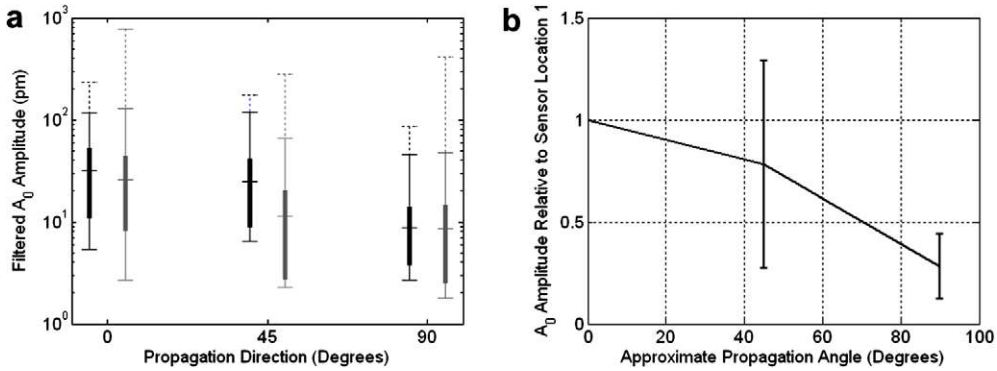

Fig. 12. Angular amplitude patterns from delamination events: (a) mean amplitude, amplitude range and standard deviation of waveforms from specimen DL-L-12 (black bars) and DL-L-25 (grey bars); (b) results from specimen DL-L-12 with amplitude normalized in the 0° propagation direction. The dotted lines in (a) indicate the amplitude of the largest 10 events which are excluded from the calculations of mean and standard deviation.

the plots using dotted lines. It can be seen that the angular amplitude pattern is less repeatable than in the matrix cracking events by comparison with Fig. 9a.

Fig. 12b shows the angular amplitude pattern obtained by normalizing the amplitude of each event by that in the 0° ply direction. It can be seen that the surface displacement varies by about 12 dB over the range of measurements. Despite some evidence of an angular amplitude pattern, the error bars, indicating the range of the normalized amplitude at each angular location, show that the pattern is not repeated for each event. No clear angular amplitude patterns were seen for delamination events in specimen DL-L-25. There are several reasons why delamination events may not exhibit any clear angular amplitude pattern. First, there may be angular variation in the radiation pattern from individual events but the events themselves may be randomly oriented. Secondly, the presence of the delaminated region itself may distort the measured angular amplitude as waves detected in different directions have to pass through different lengths of delaminated plate. This effect will depend on whereabouts in the delaminated region a particular event occurs and will change as the test progresses and the delaminated area grows. Unfortunately, there is insufficient experimental data to reliably probe any of these hypotheses further. However, regardless of the precise mechanism, the knowledge that the average angular amplitude distribution for delamination events is fairly uniform provides the necessary information for use in AE system design.

5. Discussion

5.1. Comparisons with the literature

It was noted in the introduction that most reported AE studies in the literature are conducted on narrow specimens which makes comparisons difficult. Several modal AE studies have noted that a different source orientation leads to a different S_0–A_0 amplitude ratio [6]. It has also been shown that matrix cracking events are generally dominated by the S_0 mode and delamination events are dominated by the A_0 mode [7]. In this respect, the results reported in this work are therefore in agreement with previous findings.

5.2. Implications for SHM monitoring

The primary purpose of obtaining reflection-free and absolute measurements of the AE waveforms from genuine damage mechanisms is to provide the input into forward models of AE-based SHM on real composite components with more complex geometries. In a forward model, the input is an AE source of a specified type and at a specified location, while the outputs are the waveforms received at one or more AE sensors. Such models can be based on direct numerical simulation of wave propagation (e.g. using finite elements) or more efficiently using ray-tracing approaches. In both cases, the starting point is the guided wave modal amplitudes in the experimentally-measured, reflection-free displacement waveforms. In direct simulation models, the modal amplitudes must be converted into equivalent monopole or dipole forces (e.g. using the concept of modal excitability [28]), which are then applied at any candidate source location in the modeling domain. In ray-tracing methods, the possible paths of rays from a candidate source location to each sensor must be calculated, which may include multiple reflections by or transmissions past structural features. Wavepacket propagation along each ray-path is simulated (using either experimentally-measured or model data for reflection and transmission coefficients at structural features) and the results summed to obtain the total waveform at a sensor. The ray-tracing approach is more efficient but best suited to structures with only moderate complexity (e.g. a plate stiffened with stringers) while direct numerical simulation can obviously be applied to structures of arbitrary complexity. The only requirement in either case is that the thickness of the structure at each source location should be identical to that of the plate on which the experimental data was obtained.

A forward model enables the overall performance of an AE system with sensors at specified locations to be investigated. This is done by simulating events at many locations (and many orientations if applicable) in the structure in turn and determining which of these can be detected, leading to a measure of Probability Of Detection (POD). Alternative sensor layouts and signal processing strategies can be compared using the POD and the optimum configuration to achieve a given POD can be determined.

For the detection of events with uniform angular amplitudes, the optimum sensor layout in a uniform plate structure should have approximately uniform spacing in all directions. The spacing is determined by the absolute amplitude of events, and these should be obtained from quantitative experimental measurements of the type described in this article.

The large angular amplitude pattern from matrix cracking events highlights why narrow specimens cannot be used for the derivation of even simple performance metrics. In a monitoring environment, it is likely that the location of damage is unknown, and as a result, the propagation direction between the source and sensor is unknown. The variation in the angular amplitude of the matrix cracking event has been shown to be approximately 20 dB. Thus depending on the angular position of the source rela-

tive to the sensor, the amplitude of the waveform at a sensor location will vary greatly. By including the angular amplitude patterns in a forward model, these effects can be accounted for in the design and evaluation of AE monitoring systems. If the loading direction of the structure is predominantly uni-directional, the likely orientation of possible matrix cracking can be estimated and the angular amplitude pattern of emissions is constant with respect to the structure. In this scenario, the optimum sensor layout on a uniform plate structure is a network with closer spacing in the direction of lowest angular amplitude.

The ability to distinguish between different types of damage mechanism is desirable in any SHM application and is widely debated in the AE community. Some authors report that damage can be identified using simple parameters such as amplitude whilst others find that amplitude ranges for different damage types overlap. The characteristics reported in this work suggest that the latter is true, since the amplitude of the matrix cracking and delamination events do indeed overlap. However, the two specific types of damage studied here do show distinct characteristics such as modal content and angular amplitude. These provide potential tools to discriminate between different sources of AE. These could be implemented, for example, by using software to match the measured variations in angular amplitude or modal content with the known characteristics of different AE events. This work therefore provides a starting point for specifying quantitative damage recognition based on a scientific foundation as opposed to empirical trends.

The mode-dependent source location has shown excellent agreement with independent measurements of damage. As a result, it has been shown that carefully applied source location provides another method of quantifying the damage and can be used to support deterministic SHM.

6. Conclusions

- A quantitative procedure for characterizing acoustic emission (AE) from damage in composites has been described. A key requirement is the use of relatively large specimens in order to minimize the effect of edge reflections. A procedure to determine the necessary specimen dimensions for such source characterisation experiments has been discussed.
- Source location, coupled with independent measurements of damage, has confirmed the presence of two types of damage associated with cut plies: matrix cracking and delamination. These events occur at different strain levels during increasing quasi-static loading and, as a result, their source characteristics can be examined individually.
- The two types of damage studied produced very different acoustic waveforms. Matrix cracking events were dominated by the S_0 guided wave mode in all propagation directions. Despite large variations in the overall amplitude of matrix cracking events, a very consistent angular amplitude pattern was measured.
- Delamination events were dominated by the A_0A_0 guided wave mode in all propagation directions and exhibited a large variation of approximately 40 dB in the overall amplitude of events. The presence of an angular amplitude pattern for this type of damage mechanism was less obvious than for matrix cracking events.
- The results of quantitative source characterisation of the type described here form the basic input for forward models of the complete AE process in more complex structural geometries. Forward models are essential for the design of Structural Health Monitoring (SHM) systems based on AE, and enable metrics such as Probability of Detection (POD) to be estimated for specified types of damage.
- The measured difference in the characteristics of the two sources suggests that it may be possible to apply pattern recognition techniques to identify the different types of damage occurring in a complex environment.

Acknowledgements

This work was supported by the UK Engineering and Physical Sciences Research Council (Grant No. GR/T01136/01) through the UK Research Centre in NDE and by Airbus, Rolls-Royce and Nexia Solutions.

Appendix A. Stiffness properties of quasi-isotropic AS4/8552 plate.

Laminar properties (*from* [21] *except* υ_{23})

V_f	0.6
Density	1600 kg m^{-3}
Stiffness	E_1 = 135 GPa
	E_2 = 9.5 GPa
	G_{12} = 5.00 GPa
	υ_{12} = 0.3
	υ_{23} = 0.45 (estimated)

Equivalent homogenous properties of laminate

Volume fraction	0.6
Lay-up	$[(+45, 90, -45)2, 02]_s$
Thickness	2.0 mm
Density	1600 kg m^{-3}
Stiffness	E_{xx} = 52.2 GPa, G_{xy} = 20.00 GPa, υ_{xy} = 0.309
	E_{yy} = 52.2 GPa, G_{xz} = 3.96 GPa, υ_{xz} = 0.310
	E_{zz} = 11.4 GPa, G_{yz} = 3.96 GPa, υ_{yz} = 0.310

References

[1] Achenbach JD. On the road from schedule-based non-destructive inspection to structural health monitoring. In: Proceedings of the 6th international workshop on structural health monitoring. Stanford; September 1997. p. 16–28.
[2] Hamstad MA. A review: acoustic emission, a tool for composite materials studies. Exp Mech 1986;26(1):7–13.
[3] Drouillard TF. A history of acoustic emission. J Acoust Emiss 1996;14(1):1–34.
[4] Scruby CB, Baldwin GR, Stacey KA. Characterisation of fatigue crack extension by quantitative acoustic emission. Int J Fract 1985;28:210–22.
[5] Kim KY, Sachse W. Characteristics of an acoustic emission source from a thermal crack in glass. Int J Fract 1986;31:211–31.
[6] Gorman MR, Prosser WH. AE Source Orientation by plate wave analysis. J Acoust Emiss 1991;9(4):283–8.
[7] Surgeon M, Wevers M. Modal analysis of acoustic emission signals from CFRP laminates. NDT&E Int 1999;32:311–22.
[8] Gorman MR, Ziola SM. Plate waves produced by transverse matrix cracking. Ultrasonics 1991;29:245–51.
[9] Prosser WH, Jackson KE, Kellas S, Smith BT, McKeon J, Friedman A. Advanced, waveform based acoustic emission detection of matrix cracking in composites. Mater Eval 1995;53(9):1052–8.
[10] Scholey JJ, Wilcox PD, Lee CK, Friswell MI, Wisnom MR. Acoustic emission in wide composite specimens. In: Proceedings of the 27th European conference on acoustic emission testing. Cardiff; September 2006. p. 325–332.
[11] Schmerr LW. Fundamentals of ultrasonic non-destructive evaluation. A modeling approach. New York: Plenum Press; 1998.
[12] Standard method for primary calibration of acoustic emission sensors. ASTM Standard E1106.
[13] Jacobs LJ, Woolsey CA. Transfer functions for acoustic emission transducers using laser interferometry. J Acoust Soc Am 1993;94(6):3506–8.
[14] Hatano H, Mori E. Acoustic-emission transducer and its absolute calibration. J Acoust Soc Am 1976;59(2):344–9.
[15] Tobias A. Acoustic-emission source location in two dimensions by an array of three sensors. Non-Destr Test 1976;9:9–12.
[16] Kurokawa Y, Mitzutani Y, Mayuzumi M. Real-time executing source location system applicable to anisotopric thin structures. J Acoust Emiss 2005;23:224–32.

[17] Scholey JJ, Wilcox PD, Wisnom MR, Friswell MI. Two-dimensional source location techniques for large composite plates. In: Proceedings of the 28th European conference on acoustic emission testing. Krakow; September 2008. p.160–165.
[18] Hamstad MA, O'Gallagher A, Gary J. Effects of lateral plate dimensions on acoustic emission signals from dipole sources. J Acoust Emiss 2001;19:258–69.
[19] Viktorov IA. Rayleigh lamb waves physical theory and applications. New York: Plenum Press; 1967.
[20] Gorman MR. Some connections between AE testing of large structures and small samples. Nondestruct Test Eval 1998;14(1):89–104.
[21] Giglotti M, Wisnom MR, Potter KD. Loss of bifurcation and multiple shapes of thin [0/90] unsymmetric composite plates subject to thermal stress. Compos Sci Technol 2004;64:109–28.
[22] Sachse W, Pao YH. On the determination of phase and group velocities of dispersive waves in solids. J Appl Phys 1978;49(8):4320–7.
[23] Palakovic B, Lowe MJS. DISPERSE: a system for generating dispersion curves, User's Manual. Imperial College, London; 2000.
[24] Wilcox PD, Lowe M, Cawley P. The effect of dispersion on long-range inspection using ultrasonic guided waves. NDT&E Int 2001;34:1–9.
[25] Cui W, Wisnom MR, Jones M. An experimental and analytical study of delamination of unidirectional specimens with cut central plies. J Reinf Plast Compos 1994;13:722–39.
[26] Tian Z, Swanson SR. The fracture behaviour of carbon/epoxy laminates containing internal cut fibres. J Compos Mater 1991;25:1427–44.
[27] Towse A, Setchell CJ, Potter KD, Clarke AB, Macdonald JHG, Wisnom MR, Adams RD. Use experience with a developmental general purpose non-contacting extensometer with high resolution. ASTM Special Technical Publication 1323; 2001. p. 36–51.
[28] Velichko A, Wilcox PD. Modeling the excitation of guided waves in generally anisotropic multi-layered media. J Acoust Soc Am 2007;121(1):60–9.